PROTEIN ROTATIONAL MOTION IN SOLUTION MEASURED BY POLARIZED FLUORESCENCE DEPLETION

THOMAS M. YOSHIDA AND B. GEORGE BARISAS
Department of Chemistry, Colorado State University, Fort Collins, Colorado 80523

ABSTRACT A microscope-based system is described for directly measuring protein rotational motion in viscous environments such as cell membranes by polarized fluorescence depletion (PFD). Proteins labeled with fluorophores having a high quantum yield for triplet formation, such as eosin isothiocyanate (EITC), are examined anaerobically in a fluorescence microscope. An acousto-optic modulator generates a several-microsecond pulse of linearly polarized light which produces an orientationally-asymmetric depletion of ground state fluorescence in the sample. When the sample is then probed with light polarized parallel to the excitation pulse, fluorescence recovers over 0–1,000 μs as the sum of two exponentials. One exponential corresponds to triplet decay and the other to the rotational relaxation. An exciting pulse perpendicular to the probe beam is then applied. Fluorescence recovery following this pulse is the difference of the same two exponentials. Equations for fluorescence recovery kinetics to be expected in various experimentally significant cases are derived. Least-squares analysis using these equations then permits the triplet lifetime and rotational correlation time to be determined directly from PFD data. Instrumentation for PFD measurements is discussed that permits photobleaching recovery measurements of lateral diffusion coefficients using the same microscope system. With this apparatus, both rotational and translational diffusion coefficients (D_r, D_t) were measured for EITC-labeled bovine serum albumin in glycerol solutions. Values obtained for D_r and D_t are discussed in light of both the PFD models and the experimental system.

INTRODUCTION

Measurements of protein and lipid motions in biological membranes have yielded important insights into the role of membrane molecular dynamics in regulation of cell activation, transmembrane transport, and enzyme activity (McConnell, 1975; Edelman, 1976). However, the unique nature of biological systems places stringent requirements on the techniques that can be used to measure such motions. In particular, measurements must be made at or near physiological conditions, the measurements must not significantly perturb the system, and the technique must be sensitive enough to allow measurements to be made on individual cells. This later requirement arises from the necessity of examining cells with particular morphological or functional attributes among heterogeneous populations.

To date most studies of membrane molecular motions have focused on lateral diffusion using techniques such as fluorescence photobleaching recovery (FPR).[1] FPR has been applied to measurements of protein and lipid diffusion in many types of cells and artificial bilayer membranes (for a review of FPR, see Peters, 1981). One significant limitation of lateral diffusion measurements, in general, is the relative insensitivity of this type of motion to the size and shape of the diffusing particle (Peters and Cherry, 1982). For particles diffusing in three dimensions, the translational diffusion coefficient is inversely proportional to the radius of the particle, as shown in Eq. 54. According to the Saffman-Delbrück treatment for particles constrained to a two-dimensional system (Saffman and Delbrück, 1975; Saffman 1976), an even weaker dependence on the logarithm of the particle radius is predicted. On the other hand the rotational diffusion coefficient is inversely proportional to the volume of the rotating particle (Eq. 53). Moreover, rotational diffusion is highly sensitive to molecular asymmetry. This type of measurement is thus potentially much more sensitive to size and shape factors. Considerable interest has therefore arisen in the development of techniques to measure rotational diffusion of membrane components and applications of rotational motion measurements have been reviewed by Garland and Johnson (1985).

A technique that shows promise for determining slow rotational motions on single cells was first introduced by Johnson and Garland (1981). This technique, which we call Polarized Fluorescence Depletion (PFD), takes advantage of the high sensitivity of fluorescence detection and utilizes the extended lifetime of the exicted triplet state. This allows measurement of rotational motions as slow as a

Please address all correspondence to Dr. Barisas.

[1] *Abbreviations used in this paper:* PFD, polarized fluorescence depletion; FPR, fluorescence photobleaching recovery; BSA, bovine serum albumin; EITC, eosin-5'-isothiocyanate; diI, 3,3'-dioctadecylindocarbocyanine iodide; AOM, acousto-optic modulator; MCS, multichannel scalar.

few milliseconds. In this technique a protein is labeled with a fluorescent dye such as eosin isothiocyanate (EITC) which has a significant quantum yield for triplet formation. A brief pulse of linearly polarized light preferentially excites to the triplet state molecules whose absorption dipoles are aligned parallel to the exciting pulse. This produces an orientationally asymmetric depletion of ground state molecules. Fluorescence excited by a low-powered probe beam is thus reduced in magnitude and partially polarized after the high powered pulse. Recovery of fluorescence after depletion is dependent on both triplet decay and rotational relaxation. By alternately monitoring recovery of fluorescence excited by light polarized parallel and perpendicular to the polarization of the depletion pulse, both the triplet lifetime and rotational relaxation time can be determined. Wegener (1984) has derived the theoretical basis for PFD measurements in solution with various combinations of depletion beam, probe beam, and detector angles. Theoretical treatment of microscope-based systems using epiillumination and treatment of cellular samples have yet to be considered.

We have developed a system similar to that of Johnson and Garland and incorporated it into our existing FPR system (Peacock and Barisas, 1981). This allows the measurement of both rotational and translational diffusion under very similar experimental conditions. A new approach for analyzing PFD data has also been employed. Equations that describe PFD fluorescence recovery kinetics in four experimentally important geometries have been derived. These are: (*a*) rotation of spherical particles in a three-dimensional isotropic medium; (*b*) rotation of particles in an infinite plane; (*c*) rotation of particles in a spherical surface; and (*d*) rotation normal to the surface of a sphere of particles labeled with randomly oriented fluorophores. The first case corresponds to the motion of a spherical molecule in solution. The second case applies to the rotation of a molecule like 3,3'-dioctadecylindocarbocyanine iodide (diI) in a planer bilayer. The third case represents diI motion in cells or vesicles observed completely. The last case most closely describes the general rotational motion of a uniformly fluorochrome-labeled protein in a cell membrane. Nonlinear least suqares analysis using the above equations then permits the rotational correlation time and triplet lifetimes to be evaluated directly from PFD data. Initial and residual anisotropies can also be evaluated by the same procedure. Correction factors that take into account high numerical aperture observation are discussed, as are equations describing laser—induced sample heating in both solution and cellular studies. We describe our PFD optical system and the various refinements it contains. Finally, experimental measurements of the determination of both translational and rotational diffusion of bovine serum albumin (BSA) in glycerol are reported. These experiments show that PFD methods provide reliable determinations of protein rotational correlation times.

GLOSSARY

τ_t	triplet lifetime
τ_r	rotational correlation time
$I_{\parallel}$	parallel fluorescence intensity
$I_{\perp}$	perpendicular fluorescence intensity
I_0	pre-depletion fluorescence intensity
$\vec{E}$	excitation light electric vector
$\vec{\mu}$	fluorophore absorption dipole
$S(\theta, \phi, t)$	ground state singlet distribution function
$T(\theta, \phi, t)$	triplet distribution function
θ, ϕ, ψ, ξ	sample coordinate angles
P_0, P_2, P_4	zero, second, and fourth order Legendre polynomials
$B/3$	fractional ground state depletion
S_0	total number of ground state molecules
I	source intensity
λ	wavelength of light
ϵ	molar absorptivity
Φ_t	quantum yield for triplet formation
ℓ	sample path length
h	Plank's constant
c	speed of light
Δt	duration of depletion pulse
D_r, D_t	rotational and translational diffusion coefficients
k_ℓ	first order rate constant for triplet decay
$\vec{\mu}_x, \vec{\mu}_y, \vec{\mu}_z$	$(\vec{\mu} \cdot \vec{x}), (\vec{\mu} \cdot \vec{y}), (\vec{\mu} \cdot \vec{z})$, respectively
k_c	combined rate constant: $6D_r + k_\ell$ or $4D_r + k_\ell$
σ_0	collection half angle
NA	numerical aperture
n	index of refraction
κ	thermal diffusivity of sample
κ_0	thermal diffusivity of cover glass and slide
$\dot{q}$	rate of heat production
ρ	sample density
c_p	sample specific heat capacity
w	laser beam $1/e^2$ radius
P_t	total laser power incident on sample
γ	Euler's number = 0.577 . . .
T_∞	excess temperature at $z = 0$ and $r = 0$, in cylindrical sample
T_{surf}	excess temperature at the surface of spherical laminar
N	Avogadro's number
n_f	number of fluorophores on a spherical surface
k	Boltzmann's constant
η	viscosity
r	hydrodynamic radius of particle
e	2.71828 . . .

THEORY

The concept of PFD measurement of macromolecular rotation is shown in Fig. 1. Spherical molecules, each containing a single rigidly attached fluorophore, are observed in a viscous environment. A low intensity vertically polarized probe beam initially irradiates the sample for ~100 μs to determine initial steady-state fluorescence intensity. Next, an acousto-optic modulator (AOM) is activated to produce a light pulse approximately 100 times as intense as the probe beam. This pulse is vertically polarized and preferentially absorbed by those molecules whose absorption transition dipoles are aligned vertically (Fig. 1 *left*). The sample is anaerobic and the ground state is therefore anisotropically depleted by triplet formation. When the probe beam is again applied to the sample, the fluorescence intensity is decreased relative to the pre-

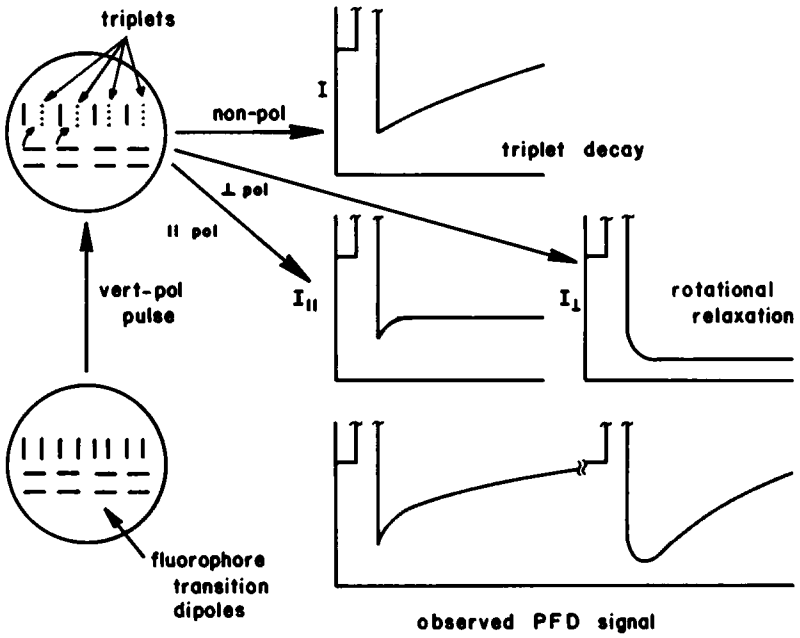

FIGURE 1 Measurement of protein rotational diffusion by polarized fluorescence depletion (PFD). The figure in the *upper right* shows the fluoresence recovery via triplet decay only which is observed upon fluorescence excitation with nonpolarized light. The figures at *right center* illustrate (on a more rapid timescale) fluorescence recovery via rotational relaxation observed when fluorescence is excited with light linearly polarized either parallel or perpendicular to the depletion pulse. The figure at the *lower right* illustrates PFD data as observed where fluorescence recovery occurs via both mechanisms simultaneously.

depletion level. Recovery of fluorescence after the first depletion pulse occurs by two mechanisms. The first is triplet decay to the ground state which results in an exponential increase with time of the fluorescence intensity (Fig. 1 upper right), as determined by the triplet lifetime τ_ℓ. The second mechanism is rotational relaxation of fluorescent ground state molecules into the depleted orientation (Fig. 1 right center). This yields an exponential *increase* with time in fluorscence, as governed by the rotational correlation time τ_r. After fluorescence has recovered nearly to its pre-depletion value, data collection is halted long enough to allow complete recovery of the ground state. The pulse-probe cycle is then repeated a second time except that the probe beam is now horizontally polarized. The recovery of fluorescence intensity following the pulse will depend on the same two exponentials as in the first cycle. Triplet decay will again cause fluorescence to increase with time. However, since fluorescence from horizontally oriented molecules is now monitored, rotational relaxation of ground state fluorophores into the depleted orientation will cause a *decrease* with time in the fluorescence intensity (Fig. 1 right center). Therefore, in the first cycle one monitors recovery of fluorescence (I_{II}) excited by a probe parallel to the depletion pulse. I_{II} is the *sum* of two exponentials (Fig. 1 lower right). In the second cycle, recovery of fluorescence ($I_\perp$) excited by a probe perpendicular to the depletion pulse is monitored, and this quantity is the *difference* of the same two exponentials.

We develop below simple equations that predict the absolute fluorescence recovery signals observed in PFD experiments. These equations are for use in analyzing PFD experimental data and the complexity appropriate in such models is therefore limited by the attainable precision of such data. For example, the amount of molecular rotational information obtainable from the membrane of a single cell is necessarily quite limited. If the equations describing PFD recovery kinetics contain too many adjustable parameters, difficulties in evaluating any single parameter, for example, the rotational correlation time, will be greatly increased. The simplest possible descriptions of macromolecular rotation therefore seem indicated for this specific application. In the derivations below we consider particles containing a single rigidly attached fluorophore, whose triplet state decays as a single exponential and whose fluorescence lifetime is much shorter than its rotational correlation time. In all cases we take the absorption and fluorescence emission transition dipoles to be parallel one to another. This has been shown to be a reasonable assumption for EITC (Cherry et al., 1976) and erythrosin (Speire et al., 1983), which are the fluorophores of greatest interest in these experiments.

Rotation of a Sphere in Three Dimensions

A spherically symmetric particle, rigidly labeled with a single fluorophore and free to rotate in an isotropic medium, is placed at the origin of a fixed x, y, z laboratory coordinate system (Fig. 2 a), where $\vec{\mathbf{i}}$, $\vec{\mathbf{j}}$ and $\vec{\mathbf{k}}$ are unit

vectors along the x, y and z-axes, respectively. The excitation light travels along the x-axis and is polarized with its electric vector $\vec{E}$ parallel to the z-axis. The duration of the excitation pulse is short relative to both the triplet lifetime and the rotational relaxation. The orientation of the rigidly attached absorption transition dipole moment $\vec{\mu}$ is described by the angles θ and ϕ with respect to the fixed coordinate system.

We let $S(\theta, \phi, t)$ and $T(\theta, \phi, t)$ equal the time-dependent distribution functions for ground state singlets and excited triplets, respectively. The probability that a ground state molecule will absorb light and be excited to the triplet state is proportional to $(\vec{\mu} \cdot \vec{E})^2$, therefore the initial distribution of excited molecules is proportional to $\cos^2 \theta$. Given that the fraction of ground state molecules excited in any given pulse is small, the initial normalized distribution for triplets and excited singlets immediately after the depletion pulse is

$$\frac{T(\theta, \phi, 0)}{S_0} = \frac{1}{4\pi}\left[\frac{B}{3} P_0(\cos\theta) + \frac{2B}{3} P_2(\cos\theta)\right] \quad (1)$$

and

$$\frac{S(\theta, \phi, 0)}{S_0} = \frac{1}{4\pi}\left[1 - \frac{B}{3} P_0(\cos\theta) - \frac{2B}{3} P_2(\cos\theta)\right] \quad (2)$$

where $B/3$ is the total fractional ground state depletion, S_0 is the total number of molecules, and P_0 and P_2 are Legendre polynomials in $\cos\theta$. For an excitation pulse that is short in comparison both to the triplet lifetime and to the rotational relaxation time, B, is given by

$$\frac{B}{3} = \frac{2.303 I \epsilon \lambda}{hcN} \Phi_t \Delta t, \quad (3)$$

where I is the intensity of the depletion pulse, λ is the wavelength of light, ϵ is the molar absorptivity for the fluorophore, Φ_t is the quantum yield for triplet formation, N is Avogardo's number, c the speed of light, h is Planck's constant and Δt is the duration of the depletion pulse. The time-dependent distribution functions must also satisfy the rotational diffusion equation. Assuming there are no dimensional restrictions to rotational motion,

$$\frac{\partial T(\theta, \phi, t)}{\partial t} = D_r \nabla^2 T(\theta, \phi, t) - k_\ell T(\theta, \phi, t) \quad (4)$$

and

$$\frac{\partial S(\theta, \phi, t)}{\partial t} = D_r \nabla^2 S(\theta, \phi, t) + k_\ell T(\theta, \phi, t) \quad (5)$$

where $D_r = 1/6\tau_r$. The second term in Eqs. 4 and 5 is the contribution due to triplet decay, for which process k_ℓ is the first order rate constant. The time-dependent distribution functions are evaluated as sums of Legendre polynomials by standard methods. If we equate k_ℓ with $1/\tau_\ell$, the ground state distribution function can be written as

$$\frac{S(\theta, \phi, t)}{S_0} = \frac{1}{4\pi}\left\{1 - \frac{B}{3} P_0(\cos\theta) \exp\left(-\frac{t}{\tau_\ell}\right) - \frac{2B}{3} P_2(\cos\theta) \exp\left[-\left(\frac{1}{\tau_\ell} + \frac{1}{\tau_r}\right) t\right]\right\}. \quad (6)$$

To calculate the experimentally observed fluorescence intensity, we recall that the fluorescence emission transition dipole moment was assumed parallel to the absorption transition dipole. Therefore the intensity of fluorescence emitted upon excitation with light polarized parallel to the z-axis is proportional to $(\vec{\mu} \cdot \vec{k})^2$. This probability is multiplied by the fraction of molecules at each orientation (Eq. 6) and the integral taken over all angular coordinates. Therefore,

$$I_{\parallel} = 3 I_0 \iint \cos^2\theta \, S(\theta, \phi, t) \, d\Omega, \quad (7)$$

where $d\Omega = \sin\theta \, d\theta \, d\phi$. I_0 is the pre-depletion fluorescence intensity given by:

$$I_0 = 2.303 \epsilon C \ell I \Phi_f E_f, \quad (8)$$

where Φ_f is the quantum yield for fluorescence, E_f is the detector fluorescence collection efficiency, C is the molar concentration, and ℓ is the sample path length. Substituting Eq. 6 and integrating gives

$$I_{\parallel} = I_0\left\{1 - \frac{B}{3}\exp\left(-\frac{t}{\tau_\ell}\right) - \frac{4B}{15}\exp\left[-\left(\frac{1}{\tau_\ell} + \frac{1}{\tau_r}\right) t\right]\right\}. \quad (9)$$

Similarly, the probability for emission being detected parallel to the y-axis is proportional to $(\vec{\mu} \cdot \vec{j})^2$. Therefore the fluorescence intensity observed in this orientation is

$$I_{\perp} = 3 I_0 \iint \cos^2\phi \sin^2\theta \, S(\theta, \phi, t) \, d\Omega. \quad (10)$$

Substituting and integrating gives

$$I_{\perp} = I_0\left\{1 - \frac{B}{3}\exp\left(-\frac{t}{\tau_\ell}\right) + \frac{2B}{15}\exp\left[-\left(\frac{1}{\tau_\ell} + \frac{1}{\tau_r}\right) t\right]\right\}. \quad (11)$$

Fluorescence Detection with Polarization Analyzer

When a polarization analyzer is placed ahead of the detector, polarized fluorescence can be measured in various topologically distinct experimental configurations. These configurations correspond to the relative polarizations of the depletion pulse (always propagating along the x-axis and polarized in the z-direction), the probe beam (also propagating along the x-axis and polarized in either the z- or y-directions), and the polarization analyzer (either located along the x-axis and z- or y-polarized or located along the y-axis and x-polarized). Three configurations exist where the polarization of the probe beam is

parallel to that of the depletion pulse. Fluorescence emission can be monitored along the x-axis with the analyzer either parallel to the depletion beam $I_{(\parallel,\parallel)}$ or perpendicular to the depletion beam $I_{(\parallel,\perp)}$. Alternatively, emission can be measured along the y-axis with the analyzer parallel to the x-axis $I_{(\parallel,x)}$. Three other orientations correspond to emission probed perpendicular to the depletion pulse with the analyzer in the same configurations described above. The measured fluorescence emission intensities are then $I_{(\perp,\parallel)}$, $I_{(\perp,\perp)}$, and $I_{(\perp,x)}$, respectively. The following equations describe the various observed intensities for the case of isotropic three dimensional rotation, where the following notation is used: $\vec{\mu}_z = (\vec{\mu} \cdot \vec{k})$, $\vec{\mu}_y = (\vec{\mu} \cdot \vec{j})$ and $\vec{\mu}_x = (\vec{\mu} \cdot \vec{i})$.

$$I_{(\parallel,\parallel)} = 3I_0 \iint \vec{\mu}_z^2 \vec{\mu}_z^2 S(\theta, \phi, t)\, d\Omega \tag{12}$$

$$I_{(\parallel,\perp)} = 3I_0 \iint \vec{\mu}_z^2 \vec{\mu}_y^2 S(\theta, \phi, t)\, d\Omega \tag{13}$$

$$I_{(\parallel,x)} = 3I_0 \iint \vec{\mu}_z^2 \vec{\mu}_x^2 S(\theta, \phi, t)\, d\Omega \tag{14}$$

$$I_{(\perp,\parallel)} = 3I_0 \iint \vec{\mu}_y^2 \vec{\mu}_z^2 S(\theta, \phi, t)\, d\Omega \tag{15}$$

$$I_{(\perp,\perp)} = 3I_0 \iint \vec{\mu}_y^2 \vec{\mu}_y^2 S(\theta, \phi, t)\, d\Omega \tag{16}$$

$$I_{(\perp,x)} = 3I_0 \iint \vec{\mu}_y^2 \vec{\mu}_x^2 S(\theta, \phi, t)\, d\Omega \tag{17}$$

The results of the integrations are given in Table I. As would be expected, the different orientations of the polarization analyzer affect only the preexponential terms in the recovery kinetics equations. We also note the sum of intensities observed in the three different orientations reduces to the intensity observed without an analyzer present (Eqs. 9 and 11), as would be required by symmetry. Table I shows that, of all possible pairs of measurement geometries, A_3 differs most between $I_{(\parallel,\parallel)}$ and $I_{(\perp,\perp)}$ while A_2 remains the same. This pair thus provides the maximum kinetic information for resolving the rates of rotational relaxation and triplet recovery. Fortuitously, both these configurations can be realized in a microscope optical system which can be shifted from one configuration to the other by a single Pockels cell. These geometries are thus used to obtain all data reported here. Equations for $I_{(\parallel,\parallel)}$ and $I_{(\perp,\perp)}$ also appear in Table II where recovery kinetics for all the four models we developed are compared.

TABLE I
PFD FLUORESCENCE RECOVERY KINETICS FOR ROTATION OF A SPHERICAL PARTICLE IN THREE DIMENSIONS

	A_1	A_2	A_3
$I_{(\parallel,\parallel)}$*	3/5	1/5	8/35
$I_{(\parallel,\perp)}$	1/5	1/15	2/105
$I_{(\parallel,x)}$	1/5	1/15	2/105
$I_{(\perp,\parallel)}$	1/5	1/15	2/105
$I_{(\perp,\perp)}$	3/5	1/5	−4/35
$I_{(\perp,x)}$	1/5	1/15	−4/105

*For all indicated intensities I, $I = I_0[A_1 - A_2 B \exp(-k_t t) - A_3 B \exp(-k_c t)]$, where $k_c = 6D_r + k_t$. The meanings of the various subscripts attached to the intensities are given in the text.

Addition of a polarization analyzer can, in theory, complicate observed fluorescence recovery kinetics. When the extent of triplet conversion is not negligibly small, i.e. $B \approx 1$, the initial ground state distribution function in Eq. 2 will contain a term $(8B^2/35)\, P_4(\cos\theta)$. In the absence of a polarization analyzer, such a higher-order Legendre term does not give rise to observable fluorescence signals. When an analyzer is present, the instrument response to the distribution function contains terms in $P_4(\cos\theta)$. The fluorescence recovery kinetics then contain rapid rotational terms of the form $\exp[-(k_t + 20D_r)t]$. However, even for B as large as 1.0, these rapid terms have very small amplitudes, only 3.8% of the total rotational recovery amplitude in $I_{(\parallel,\parallel)}$. Thus the calculations presented here are applicable without modification to the highest extents of triplet conversion that can be achieved in practice.

Rotation Observed in an Infinite Plane

We consider a particle in a two-dimensional plane rotating about the normal to the plane. The particle is located at the origin of the coordinate system, where the single, rigidly

TABLE II
PFD FLUORESCENCE RECOVERY KINETICS FOR VARIOUS GEOMETRIES

Model		A_1*	A_2	A_3
Spherical molecule in three dimensions				
no polarizer	$I_\parallel$	1	1/3	4/15
	$I_\perp$	1	1/3	−2/15
with polarizer	$I_{(\parallel,\parallel)}$	3/5	1/5	8/35
	$I_{(\perp,\perp)}$	3/5	1/5	−4/35
Molecule in infinite plane				
no polarizer	$I_\parallel$	1	1/2	1/4
	$I_\perp$	1	1/2	−1/4
with polarizer	$I_{(\parallel,\parallel)}$	3/4	3/8	1/4
	$I_{(\perp,\perp)}$	3/4	3/8	−1/4
Molecule in spherical surface observed completely				
no polarizer	$I_\parallel$	1	2/5	1/5
	$I_\perp$	1	3/10	−1/10
with polarizer	$I_{(\parallel,\parallel)}$	3/5	9/35	6/35
	$I_{(\perp,\perp)}$	3/5	6/35	−3/35
Protein in a cell membrane				
no polarizer	$I_\parallel$	1	29/75	8/75
	$I_\perp$	1	23/75	−4/75
with polarizer	$I_{(\parallel,\parallel)}$	3/5	903/3675	336/3675
	$I_{(\perp,\perp)}$	3/5	651/3675	−168/3675

*For all intensities I, $I = I_0[A_1 - A_2 B \exp(-k_t t) - A_3 B \exp(-k_c t)]$ in all cases except molecular rotation in an infinite plane. In this case I_0 is replaced by $(3/2)\, I_0$ as described in the text. The quantity k_c denotes $6D_r + k_t$ for rotation in three dimensions and $4D_r + k_t$ for rotation in two dimensions.

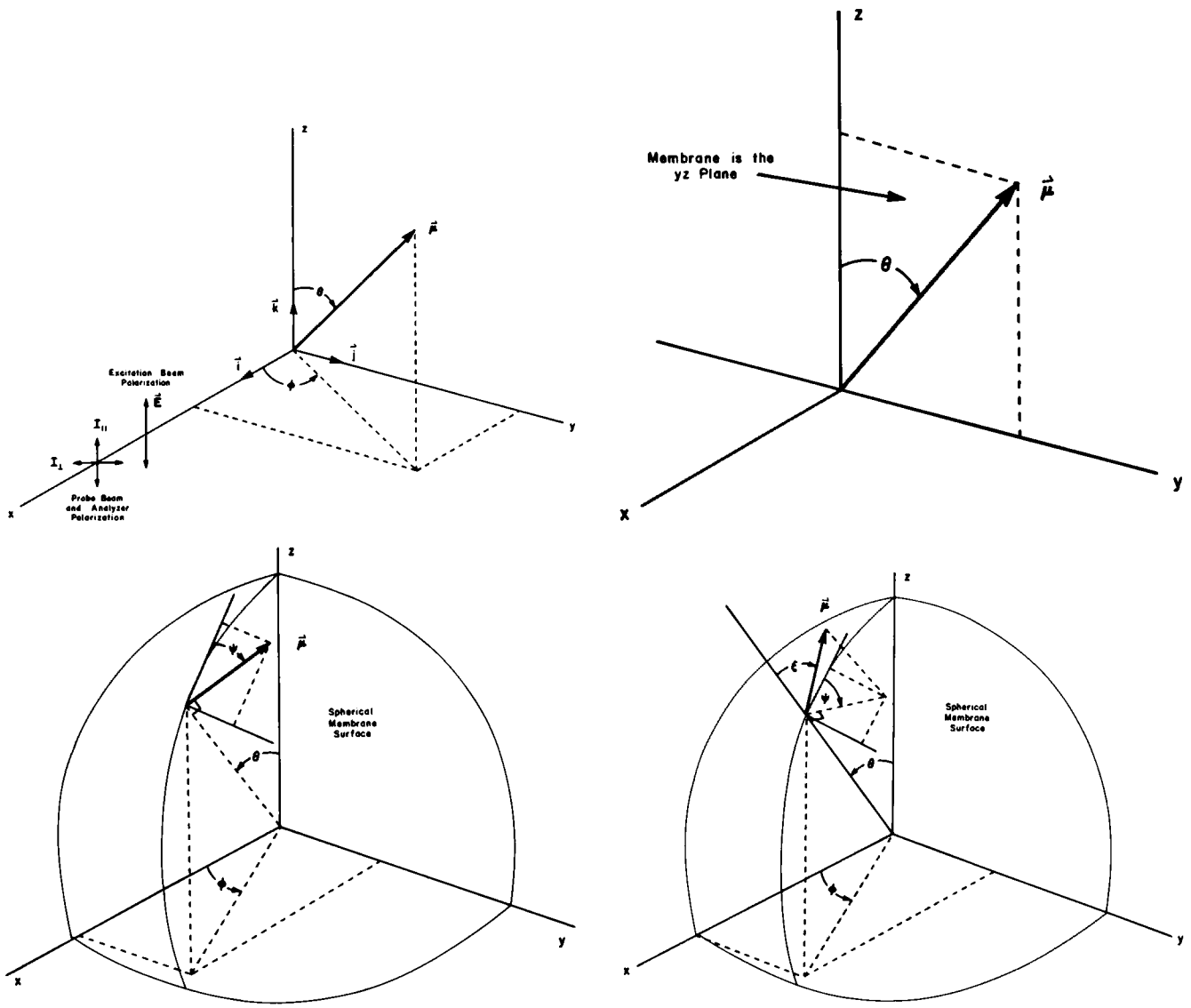

FIGURE 2 Coordinate axis for the mathematical models described in the text. In all cases the x-axis is the optical axis and the exciting light is polarized along the z-axis. (*a*) Rotation of a sphere in three dimensions. The particle is placed at the center of the x, y, z coordinate system and the transition dipole orientation is described by angles θ and ϕ. (*b*) rotation of a molecule in a plane. The transition dipole lies in the yz-plane. (*c*) rotation of particles distributed over a spherical surface observed completely. The position of the particle in the membrane is described by angles θ and ϕ and orientation of the transition dipole is described by angle ψ. (*d*) Rotation of a dye-labeled protein in a cell membrane. Angles θ, ϕ, and ψ are the same as in *c*. The additional angle ξ allows the transition dipole to lie outside the plane of the membrane.

attached transition dipole lies in the yz-plane at an angle θ to the z-axis (Fig. 2 *b*). One should note that the term θ, which is otherwise reserved for the polar angle, denotes in this case the angle of azimuthal rotation. This model corresponds to a molecule like diI confined to a planer bilayer and observed at normal incidence. The initial distributions immediately after a depletion pulse are

$$\frac{T(\theta, 0)}{S_0} = \frac{B}{2\pi}\cos^2\theta \tag{18}$$

and

$$\frac{S(\theta, 0)}{S_0} = \frac{1}{2\pi}(1 - B\cos^2\theta). \tag{19}$$

As before solution of the rotational diffusion equation given the above boundary conditions yields the time-dependent ground state distribution function as

$$\frac{S(\theta, t)}{S_0} = \frac{1}{2\pi}\left\{1 - \frac{B}{2}\exp(-k_\ell t) - \frac{B}{2}\cos 2\theta \exp(-k_c t)\right\}, \tag{20}$$

where, in the case of rotation in two dimensions, $k_c = 4D_r + k_\ell$. The fluorescence intensity observed with excitation parallel to the depletion pulse is then

$$I_{\parallel} = 2 * \frac{3}{2} I_0 \int \cos^2\theta\, S(\theta, t)\, d\theta. \tag{21}$$

The factor ⅔ arises because the molar absorptivity in I_0 is determined for particles randomly oriented in three dimensions while the molecules considered here have their transition dipoles confined to a plane. Substituting for $S(\theta, t)$ and integrating yields,

$$I_{\parallel} = \frac{3}{2} I_0 \left\{ 1 - \frac{B}{2} \exp(-k_t t) - \frac{B}{4} \exp(-k_c t) \right\}. \quad (22)$$

Similarly the fluorescence intensity observed with excitation perpendicular to the depletion pulse is

$$I_{\perp} = 2 * \frac{3}{2} I_0 \int \sin^2\theta \, S(\theta, t) \, d\theta, \quad (23)$$

which yields after integration

$$I_{\perp} = \frac{3}{2} I_0 \left\{ 1 - \frac{B}{2} \exp(-k_t t) + \frac{B}{4} \exp(-k_c t) \right\}. \quad (24)$$

Equations for $I_{(\parallel,\parallel)}$ and $I_{(\perp,\perp)}$ are evaluated by Eqs. 12 and 16, respectively, and presented in Table II.

Rotation Over a Spherical Surface Observed Completely

In this model we consider a spherical surface centered at the origin of the x, y, z coordinate system (Fig. 2 *c*). It is assumed that translational diffusion on the surface of the sphere does not occur on the rotational timescale. This model corresponds to molecules like diI confined to the surface of a spherical cell or liposome where this sphere lies completely within the region of examination. The location of a molecule in the membrane is described by angles θ and ϕ. The orientation of its transition dipole, assumed to lie in the plane of the membrane, is specified by the angle ψ between the dipole and a line joining the molecule to the intersection of the z-axis with the spherical surface (meridional line) (Fig. 2 *c*). Using the same arguments as previous, the time-dependent distribution function is

$$\frac{S(\theta, \phi, \psi, t)}{S_0} = \frac{1}{2\pi} \left\{ 1 - \frac{B}{2} \sin^2\theta \exp(-k_t t) - \frac{B}{2} \sin^2\theta \cos 2\psi \exp(-k_c t) \right\}. \quad (25)$$

The average fluorescence intensity is obtained by multiplying of the distribution function by the emission probability and integrating over both fluorophore location (θ, ϕ) and orientation (ψ). Equations describing fluorescence recovery kinetics are presented in Table II.

Rotation of a Protein in a Cell Membrane

We believe this last model most closely represents the fluorescence recovery kinetics of a protein labeled with rigidly attached, randomly oriented fluorophores and imbedded in a cell membrane. As with the previous model, the protein is constrained to rotate about an axis normal to the plane of the membrane and this rotation is described by the angle ψ defined as in the preceding case. However, unlike the previous models where the transition dipoles lie in the plane of the membrane, this model assumes a random distribution of the dipoles over angles ξ with the molecular rotational axis (Fig. 2 *d*). Absorption of light occurs preferentially for dipoles lying parallel to the z-axis. After light absorption, the angle ξ remains constant as the dipole rotates about the molecular rotation axis. The time-dependent distribution function is

$$\frac{S(\theta, \phi, \psi, \xi, t)}{S_0} = \frac{1}{2\pi} \left\{ 1 - B \left[\left(\cos^2\theta \cos^2\xi + \frac{1}{2} \sin^2\theta \sin^2\xi \right) \cdot \exp(-k_t t) + \frac{1}{2} \sin^2\theta \sin^2\xi \cos 2\psi \exp(-k_c t) \right] \right\}. \quad (26)$$

Equations describing fluorescence recovery kinetics are presented in Table II.

Anisotropy

For a variety of theoretical purposes and to assess restriction of rotational motion in membranes, the anisotropy function $r(t)$ is particularly useful. This quantity can be defined for fluorescence depletion measurements in the way suggested by Wegener (1984):

$$r(t) = \frac{\Delta I_{\parallel} - \Delta I_{\perp}}{\Delta I_{\parallel} + 2\Delta I_{\perp}}, \quad (27)$$

where:

$$\Delta I_{\parallel} = I_0 - I_{\parallel}; \quad (28)$$

$$\Delta I_{\perp} = I_0 - I_{\perp}. \quad (29)$$

The anisotropies calculated above using fluorescence depletion signals correspond to the more familiar emission anisotropies only when no polarization analyzer is used. The quantities of primary interest are r_∞, the residual anisotropy observed at infinitely long time, and r_0, the initial anisotropy observed at time zero. We modify expressions for $I_{\parallel}$ and $I_{\perp}$ so that, when $r(t)$ is calculated from Eq. 27, it has the form $r_\infty + (r_0 - r_\infty) \exp(-k_r t)$ (Jähnig, 1979). r_0 and r_∞ are then to be considered as phenomenological parameters arising from unspecified physical factors. We obtain

$$I_{\parallel} = I_0[1 - A'_{2\parallel} B \exp(-k_t t) - A'_{3\parallel} B \exp(-k_c t)]; \quad (30)$$

$$I_{\perp} = I_0[1 - A'_{2\perp} B \exp(-k_t t) - A'_{3\perp} B \exp(-k_c t)], \quad (31)$$

where

$$A'_{2\parallel} = \tfrac{1}{3} + \tfrac{2}{3} r_\infty; \quad (32)$$

$$A'_{2\perp} = \tfrac{1}{3} - \tfrac{1}{3} r_\infty; \quad (33)$$

$$A'_{3\parallel} = \tfrac{2}{3}(r_0 - r_\infty); \quad (34)$$

$$A'_{3\perp} = -\tfrac{1}{3}(r_0 - r_\infty). \quad (35)$$

These equations permit r_0 and r_∞ to be evaluated directly from PFD data by curve fitting procedures. It should be noted that, where molecules are assumed to rotate in a two-dimensional environment, there will be a nonzero residual anisotropy even in the absence of other constraints on molecular motion. Moreover, any rapid motion of the fluorophore label with respect to the protein will reduce r_0 below the expected theoretical value.

High Numerical Aperture Observation

Correction factors for high numerical aperture observations can easily be incorporated into our models using the general treatment given by Axelrod (1979). For the case of polarized observation of rotation in three dimensions, the fluorescence intensity collected by an objective is given by

$$I_{(\parallel,\parallel)} = \frac{9}{K} I_0 \iint \vec{\mu}_z^2 (K_a \vec{\mu}_x^2 + K_b \vec{\mu}_y^2 + K_c \vec{\mu}_z^2)\, S(\theta, \phi, t)\, d\Omega \quad (36)$$

and

$$I_{(\perp,\perp)} = \frac{9}{K} I_0 \iint \vec{\mu}_y^2 (K_a \vec{\mu}_x^2 + K_c \vec{\mu}_y^2 + K_b \vec{\mu}_z^2)\, S(\theta, \phi, t)\, d\Omega, \quad (37)$$

where $K = K_a + K_b + 3K_c$. The constants K_a, K_b, and K_c are functions of the objective numerical aperture (Axelrod, 1979):

$$K_a = \tfrac{1}{3}(2 - 3\cos\sigma_0 + \cos^3\sigma_0) \quad (38)$$

$$K_b = \tfrac{1}{12}(1 - 3\cos\sigma_0 + 3\cos^2\sigma_0 - \cos^3\sigma_0) \quad (39)$$

$$K_c = \tfrac{1}{4}(5 - 3\cos\sigma_0 - \cos^2\sigma_0 - \cos^3\sigma_0) \quad (40)$$

and

$$NA = n \sin\sigma_0, \quad (41)$$

where NA is the numerical aperture, n is the index of refraction of the sample, and σ_0 is the half-angle subtended by the objective. Substitution of Eq. 6 and integrating Eqs. 36 and 37 gives

$$I_{(\parallel,\parallel)} = I_0 \left\{ \frac{3}{5} - \frac{B}{5} \exp(-k_t t) - \frac{B}{5} A_1 \exp(-k_c t) \right\} \quad (42)$$

and

$$I_{(\perp,\perp)} = I_0 \left\{ \frac{3}{5} - \frac{B}{5} \exp(-k_t t) + \frac{B}{5} A_2 \exp(-k_c t) \right\} \quad (43)$$

where

$$A_1 = \frac{2K_a + 2K_b + 24K_c}{7K_a + 7K_b + 21K_c} \quad (44)$$

and

$$A_2 = \frac{4K_a - 2K_b + 12K_c}{7K_a + 7K_b + 21K_c} \quad (45)$$

For cases reported here the numerical aperture was 0.65 and the index of refraction for glycerol is 1.47. This gives values for $K_a = 1.026 \times 10^{-2}$, $K_b = 9.125 \times 10^{-5}$ and $K_c = 0.1958$. These results approach the small aperture limit described by Axelrod (1979), where $K_c \gg K_a, K_b$. In this case Eqs. 42 and 43 reduce to the noncorrected equations shown in Table I.

Laser-Induced Heating

The three dimensional samples used in fluorescence depletion measurements as described here require a treatment of laser-induced heating different from Axelrod's (1977) analysis of heating in two-dimensional photobleaching recovery samples. For the case of an isotropic solution with thermal diffusivity κ, we approximate the laser beam as a cylinder of $1/e^2$ radius r and length ℓ. The surrounding solution is considered to be infinite. The laser beam travels along the z-axis with points $\ell/2$ and $-\ell/2$ bounded by the microscope slide and cover glass, respectively, with equal thermal diffusivities of κ_0. The heating equation in cylindrical coordinates is

$$\kappa \nabla^2 T(r, t) + \dot{q}(r, t) = \rho c_p \frac{\partial T(r, t)}{\partial t}, \quad (46)$$

where $T(r, t)$ is the excess temperature, ρ is the sample density, c_p is the sample specific heat capacity, and $\dot{q}(r, t)$ is the rate of heat production.

The steady-state solution for the heating equation is

$$T(r) = \int \frac{A}{k^2} \exp(-k^2 w^2/8) \cdot \left\{ 1 - \frac{\cosh(kz)}{\cosh(k\ell/2) + (\kappa/\kappa_0)\sinh(k\ell/2)} \right\} J_0(kr)\, k\, dk, \quad (47)$$

where $J_0(kr)$ is the zero-order Bessel function, w is the laser beam $1/e^2$ radius, and A is a constant related to the beam power. For a Gaussian beam profile, A is given by

$$A = \frac{2.3\epsilon C}{2\pi\kappa} P_t, \quad (48)$$

where ϵ and C were defined previously, and P_t is the total laser power.

To simplify Eq. 47 we restrict our attention to the center of the sample where $z = 0$ and $r = 0$ and assume that $\kappa_0 = \kappa$. This is the point of highest heating and, for this location, Eq. 47 reduces to

$$T_\infty = \int \frac{A}{k^2} \exp(-k^2 w^2/8) \left[1 - \frac{1}{\exp(k\ell/2)} \right] k\, dk. \quad (49)$$

For the limiting case of a very thin sample, $w \gg \ell$ and Eq. 49 reduces to

$$T_\infty = \frac{\sqrt{\pi} A \ell}{\sqrt{2} w}. \quad (50)$$

For the case of a thick sample, $w \ll \ell$ and Eq. 49 reduces to

$$T_{00} = A\left[\ln\left(\frac{\sqrt{2}\ell}{w}\right) + \frac{\gamma}{2}\right], \tag{51}$$

where γ is Euler's number (0.577 . . .).

Typical values for the heating parameters are; $\epsilon = 10^5$ ℓ mol^{-1} cm^{-1}, $C = 3.8 \times 10^{-6}$ mol ℓ^{-1} (assuming a 1:1 protein/dye mol ratio), $\kappa = 7.0 \times 10^{-4}$ cal s^{-1} cm^{-1} °C^{-1} (for glycerol), $\ell = 0.1$ mm, $w = 25$ μm, and $P_t = 10$ mW for the high intensity, ground state depleting beam. These data give a value for the constant A of 0.48°C. Since w is the same order of magnitude as ℓ, neither of the two limiting cases applys. Therefore Eq. 49 was evaluated numerically and T_{00} was found to be 0.22°C, which is an insignificant temperature increase. The effect of the probe would also be negligible since the intensity is two orders of magnitude less than that of the depletion beam.

For a spherical cell or liposome of radius r and bearing n_f fluorophores randomly distributed over its surface, simple equations for steady-state heating (T_{surf}) at the surface can also be derived. The most important case is where the cell is illuminated by an expanded Gaussian laser spot with $1/e^2$ radius w appreciably larger than r. Solution of the thermal diffusion equation by Green's Theorem yields

$$T_{surf} = \frac{2.303\epsilon}{2\pi^2 r w^2 \kappa N} n_f P_t, \tag{52}$$

where N is Avogadro's number and all other quantities have meanings assigned earlier. For $n_f = 10^5$ fluorophores, $\epsilon = 10^5$ ℓ mol^{-1} cm^{-1}, $P_t = 10$ mW, $r = 5$ μm, $w = 5$ μm, and $\kappa = 1.4 \times 10^{-3}$ cal s^{-1} cm^{-1} °C^{-1} (for water), $T_{surf} = 0.03$°C. Clearly heating due to the depletion beam in experiments on cells or liposomes may be ignored.

METHODS AND MATERIALS

Instrumentation

The microscope-based PFD system (Fig. 3) uses a Coherent Radiation CR-4 argon ion laser (Coherent Inc., Laser Division, Palo Alto, CA) operated with a vertically polarized TEM 00 output of 100 mW at 514.5 nm. The preceding section was developed assuming the excitation beam polarization to be fixed and the probe beam polarization to rotate. However, Table II shows that the rotational component of the recovery kinetics is maximized in the total signal when the observation polarizer is kept parallel to the probe beam. It is thus most convenient to rotate the excitation beam and leave the probe beam and polarizer fixed and parallel one to the other. A Lasermetric 3031 transverse Pockels cell (Lasermetric Inc., Teaneck, NJ), driven by a special power MOSFET driver, rotates the plane of polarization of the light by 90° in <200 ns. The beam then enters a 10% beamsplitter where it is resolved into two components. The low-intensity component (probe beam) is used to monitor steady-state fluorescence. The high-intensity beam is used to excite ground state molecules to the triplet state. The probe beam, generated by reflection of light off the first surface of the beamsplitter, is attenuated with a neutral density filter before being recombined with the main beam at a second beamsplitter. The main part of the laser beam passes through the first

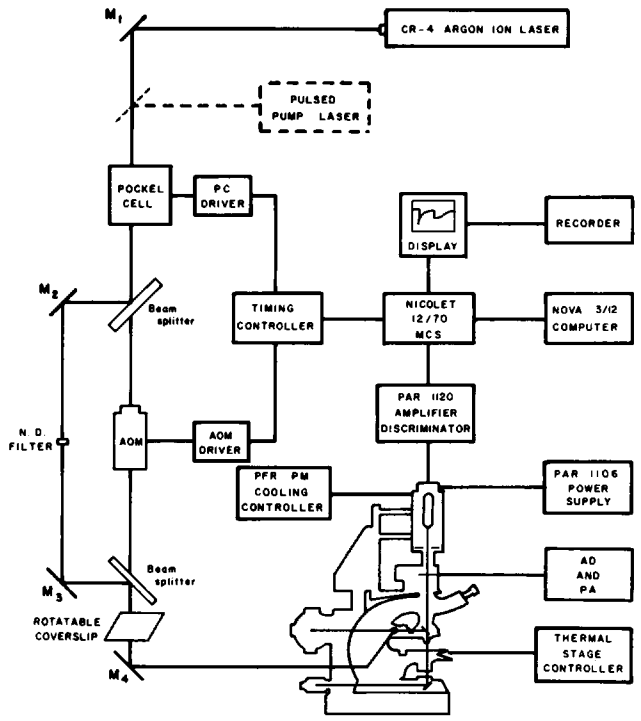

FIGURE 3 Block diagram of polarized fluorescence depletion system. M_1, M_2, M_3, M_4 are first surface mirrors, AD is an adjustable aperture diaphragm, PA is a dichroic sheet polarizer and MCS is a Nicolet 12/70 signal averager. The functions of all components are described in the text.

beamsplitter and enters a Coherent 304D acousto-optic modulator (AOM) (Coherent, Inc. Modulator Division., Danbury, CT). Pulses of 1 to 100 μs in duration are generated by isolating the first order diffracted beam of the AOM. A hardwired sequencing computer synchronizes the timing of the Pockels cell and the AOM and allows pulses of either vertical or horizontal polarizations to be generated. After recombination with the probe beam, the light passes through a microscope coverslip that is set at approximately 53° with respect to the vertical axis. The coverslip serves to compensate for intensity differences between the two orthogonal polarizations that arise from reflection off mirrors and beamsplitters. After two 90° reflections, the beam enters the lateral optical port of a Zeiss Universal microscope fitted with a III/RS epifluorescence illuminator (Carl Zeiss Inc., Thornwood, NY). For cellular studies an auxiliary lens is used in the optical port, and the laser beam has a $1/e^2$ radius of 5 μm at the sample. For solution studies, the auxiliary lens is removed, resulting in a beam radius, at the sample, of 25 μm. The beam then passes through the microscope objective and into the sample. For current studies either an X40 dry (*NA* 0.65) or an X50 water immersion fluorescence (*NA* 1.00) objective is employed. Fluorescence is collected by the objective and scattered excitation light is blocked by a dichroic mirror. Fluorescence is isolated with various combinations of glass barrier filters before entering a dichroic sheet polarizer transmitting only vertically polarized fluorescence. Light emitted from variously sized regions of the illuminated sample area is isolated by one of the aperture diaphragms of a Zeiss MP03 microscope photometer and detected with a thermionically-cooled EMI 9816A photomultiplier tube (Thorn EMI Gencom Inc., Plainview, NY), fitted with two focusing ring magnets (Products for Research Inc., Danvers, MA) to further reduce PMT dark current. A gating circuit (GB1001A, Thorn EMI Gencom Inc.) permits the PMT to be turned off during the periods of intense fluorescence emitted during the excitation pulses. Attenuation of up to 5000:1 is achieved by modifying

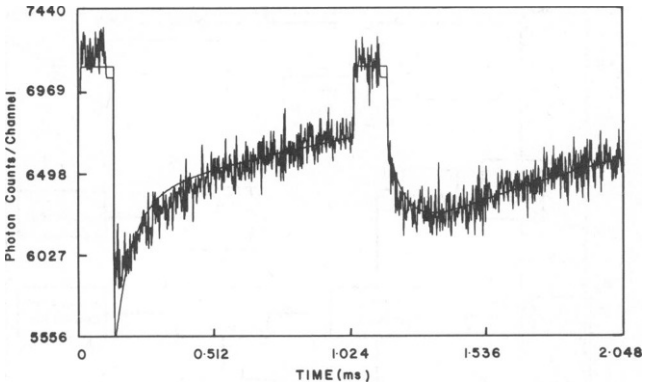

FIGURE 4 PFD data for EITC-labeled BSA in 99% glycerol at 15°C. Vertical axis is total photon counts per 2 μs channel summed over about 15,000 cycles. Horizontal axis represents time, with 2.048 msec full scale. The *left-* and *right-hand* portions of the trace represent $I_{(\parallel,\parallel)}$ and $I_{(\perp,\perp)}$, respectively. At the beginning of each portion, fluorescence was recorded for the 100 μsec preceding the depletion pulse. Because of PMT gating, fluorescence during these pulses is not visible. Between alternating $I_{(\parallel,\parallel)}$ and $I_{(\perp,\perp)}$ cycles, a 5 ms period was interposed to permit complete triplet recovery. No data were recorded during these intervals and this causes the discontinuity between fluorescence at the end of recorded $I_{(\parallel,\parallel)}$ recovery kinetics and the predepletion fluorescence of $I_{(\perp,\perp)}$. Superimposed on the raw data are fluorescence recovery curves calculated for rotation of a spherical particle in an isotropic three dimensional environment. Data analysis yields a triplet lifetime of 1.40 ms and a rotational correlation time of 65.5 μs.

the photocathode, first dynode and focusing electrode voltages from those supplied with the gating circuit. Greater attenuation is possible by further decreasing the photocathode-to-first dynode voltage, but only at the expense of limiting first dynode gain. This in turn degrades overall tube sensitivity to an unacceptable level.

Single photon counting is accomplished using a PAR 1120 amplifier/discriminator (Princeton Applied Research Corp., Princeton, NJ) modified to a 1 mV discriminator setting. The resulting ECL pulses are counted with a Nicolet 12/70 multichannel scaler (MCS) (Nicolet Inst., Madison, WI) operating in the MCS mode. When a sufficient number of counts have been accumulated by the MCS, the data are downloaded to a Nova 3/12 computer (Data General Corp., Southboro, MA). Nonlinear least squares methods are used to fit the data to appropriate models as previously described in the Theory section. Successive iterations of the fitted data are transferred back to the signal averager where they are displayed superimposed on the raw data as shown in Fig. 4.

The optical components associated with the PFD experiment are mounted on a 18" × 24" sliding optical table, which also supports the pulse generator used in the FPR experiments (Peacock and Barisas, 1981). This table is in turn mounted on a larger 4' × 8' Newport Research optical bench, (Newport, Inc., Fountian Valley, CA) on which the laser and microscope systems are also mounted. By sliding the smaller table into either of two fixed positions, the optical system used for PFD or that used for FPR can be placed in the laser beam path. Interchanging from one experimental technique to another takes only a few minutes, allowing measurements of rotational and translational diffusion to be made under very similar conditions.

Dye-Labeled Proteins

Eosin-5'-isothiocyanate (Molecular Probes, Junction City, OR) was conjugated to proteins by a method similar to that given by Cherry and Schneider (1976). Equal molar amounts of dye and protein were reacted in 0.1 M $NaHCO_3$ buffered at pH 8 and containing 0.5 m NaCl for 3–5 h at room temperature. Unreacted dye was separated on Sephadex G-25-150 and the protein was eluted with carbonate buffer. The protein solution was then dialyzed against 0.005 M phosphate buffer pH 7, lyophilyzed and stored at 0°C. To avoid photodegradation of the samples, all procedures were carried out under subdued light. The dye-to-protein molar ratio was determined by measurements of absorbance at 280 and 522 nm and, in most cases, was found to vary betweey 0.7 and 1.0.

Anaerobic solutions of BSA dissolved in glycerol were prepared by first dissolving the protein in buffer and then adding the required aliquots to anhydrous glycerol (Aldrich Gold Label, Aldrich Chemical Co., Milwaukee, WI) which had been previously bubbled with dry N_2 to remove oxygen. To maintain sample anaerobicity all manipulations were carried out in a nitrogen-filled dry box with oxygen concentrations below 1 ppm. Such anaerobic conditions apparently do not, at least in the short run, perturb the rotational dynamics of cell surface proteins. Cell viability, as measured by the fluorescein diacetate criterion, generally remains unaffected after 1 h (Damjanovich et al., 1983). More importantly, cell membrane protein rotational diffusion, as measured in time-resolved phosphorescence anisotropy experiments, apparently remains unchanged after 2–4 h exposure to anaerobic conditions, depending on the cell type (T. M. Jovin, personal communication). To reduce artifacts due to long-lived glass luminescence, the sample was placed on a quartz Supersil II microscope slide (Heraeus Amersil, Inc., Sayreville, NJ). A coverslip was sealed in place with quick-setting epoxy resin. The final concentration of protein was normally 0.2 mg/g of glycerol. The viscosity of glycerol at various concentrations and temperatures was taken from Segur and Oberstar (1951).

RESULTS AND DISCUSSION

A typical depletion and recovery trace is shown in Fig. 4 for EITC labeled BSA in 99% glycerol. 1024 data points were recorded per sweep at 2 μs per point. About 15,000 sweeps were recorded and the total counts per channel averaged 7,100. The depletion pulse had an intensity of 10 mW, a duration of 20 μs, and a beam radius of 25 μm. This produced ~10% ground state depletion. In Fig. 4 superimposed over the raw data are shown data calculated from Eqs. 12 and 16. Fitted parameters are the initial fluorescence intensity (I_0), extent of ground state depletion (B), triplet lifetime (τ_ℓ) and the rotational correlation time (τ_r). Results of the fit were I_0 = 7110 ± 9 total counts/channel, B/3 = 11.02 ± 0.15%, τ_ℓ = 1.40 ± 0.04 msec and τ_r = 66.5 ± 3.1 μs and a standard error for the overall fit of ±94 counts/channel. It is apparent that the model of a spherical particle rotating in three dimensions provides a generally satisfactory description of the data observed in this experiment. The one feature of the data not predicted by the model is the slight rounding of the beginning of the $I_{(\parallel,\parallel)}$ trace. This feature has been noted by other experimenters (P. Garland, personal communication), but the reason for its existence is unknown.

Examination of Table II shows that fluorescence recovery kinetics predicted for PFD experiments vary only slightly with the rotational model assumed. Thus consistent use of any reasonable model should satisfactorily provide the relative measurements of protein rotational relaxation times which would be desired for cell surface studies. However one major restriction must be placed on any models to be applied to cellular data. Since most membrane proteins examined to date exhibit a finite residual anisotropy, all data on such systems should be analyzed in a way which permits the residual anisotropy to

be evaluated. This is possible, for example, by the use of Eqs. 30 and 31.

Our instrumental system possesses the capability to measure both translational and rotational diffusion under similar experimental conditions. This facilitates evaluation of the performance of our rotational motion instrumentation and models. According to the Stokes-Einstein equations, both the translational and rotational diffusion coefficients are related to the hydrodynamic radius of the particle. For a spherical particle undergoing Brownian motion in a continuous medium,

$$D_r = \frac{kt}{8\pi\eta r^3} \tag{53}$$

and

$$D_t = \frac{kt}{6\pi\eta r}, \tag{54}$$

where D_t is the translational diffusion coefficient, k is Bolzmann's constant, T is the absolute temperature, η is the solvent viscosity, and r is the hydrodynamic radius of the particle. Figs. 5 *a* and 5 *b* show plots of D_r and D_t vs. T/η and demonstrate the linear dependence and zero x-intercept of both the rotational and translational diffusion as predicted by Eqs. 53 and 54. The slopes from Figs. 5 *a* and 5 *b* yield hydrodynamic radii of 32 Å from rotational measurements and 40 Å from translational diffusion measurements, respectively.

Errors associated with the technique of FPR have been discussed by Barisas and Leuther (1979) and by Barisas (1980). The most significant errors are associated with uncertainties in laser beam geometry and alignment of pulse and probe beams. It is estimated that the overall relative accuracy in measurements of D_t is ±12%. On the other hand rotational motion measurements are essentially independent of laser beam geometry; and, since an expanded beam is used for PFD measurements, the superposition of the pulse and probe beams are not critical. Other systematic errors such as differences in intensities or in the degree of polarization of the two depletion beams are insignificant compared to random errors arising from the low signal-to-noise ratios attained in these experiments. Measurements showed the degree of polarization of both depletion beams to be greater than 98% at the sample point. Also, the intensity differences of the two depletion beams can be nulled to <0.5% using the microscope coverglass mentioned previously. Therefore it is clear that counting errors limit the overall accuracy of the determination of D_r. Least-squares analysis of the data presented in Fig. 5 *b* gives an estimated relative error in D_r of ±10%.

An important consideration in both translational and rotational measurements is control of sample temperature which, along with the solvent concentration, is used to calculate η. Sample temperatures were determined by calibrating the thermally controlled microscope stage with

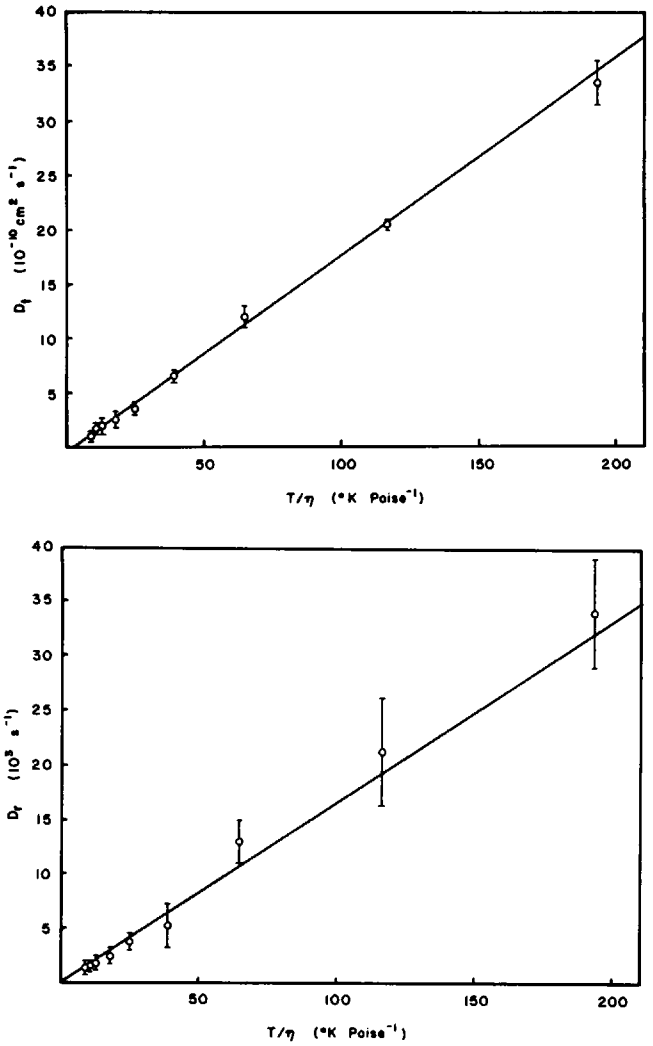

FIGURE 5 Viscosity dependence of the translational (*a*) and rotational (*b*) diffusion coefficients for EITC-labeled BSA in 99% glycerol.

a thermocouple imbedded in glycerol and placed on a microscope slide with a coverglass sealed in place. However, since both translational and rotational measurements are made on the same microscope system, we can remove both solvent viscosity and temperature dependence from the diffusion equations by plotting D_r v. D_t, yielding a slope of $3/4r^2$ and a theoretical intercept of zero. This plot (Fig. 6) gives a hydrodynamic radius for BSA of 27 Å and a y-axis intercept of $(-0.17 \pm 0.3) \times 10^3\ s^{-1}$.

From results of various hydrodynamic and spectroscopic measurements, Tanford (1961) and Kuntz and Kauzmann (1974) determined BSA is most closely approximated by a prolate ellipsoid with an axial ratio (a/b) of 2.5 to 4 and a length ($2a$) of 128 to 200 Å. Large uncertainties in these values probably arise from difficulties in evaluating the hydration and the partial specific volume of the protein, both of which are important in calculating protein size. In addition, the assumption that the protein shape is adequately approximated by a sphere or ellipsoid of revolution may not be valid or may be more critical in some experi-

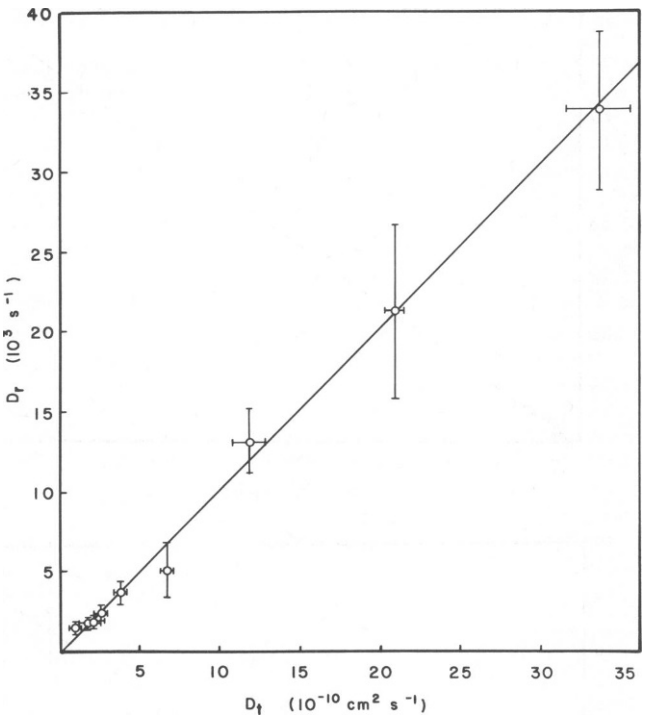

FIGURE 6 Rotational diffusion coefficient plotted versus the translational diffusion coefficient for EITC-labeled BSA in 99% glycerol. The slope is 1.029×10^{13} cm^{-2} and the y-axis intercept is -0.171×10^3 s^{-1}.

ments than others. Squires et al. (1968) report a best value for the length of BSA as 139 Å and an axial ratio of 3.5. This corresponds to a sphere of equal volume with a radius of 30 Å. Using the technique of phosphorescence anisotropy Moore et al. (1979) report a rotational diffusion coefficient of 2.38×10^3 s^{-1} for erythrosin-labeled BSA in 94% glycerol at 10°C. This value corresponds to a hydrodynamic radius of 40 Å. Using essentially the same technique as ours, Johnson and Garland (1981) reports a diffusion coefficient of 833 s^{-1} for EITC labeled BSA in 96% (wt/wt) glycerol at 2°C, implying a radius of 37 Å.

As previously mentioned, our data analysis was based on the assumption that the protein was spherical in shape. If we assume that BSA is a prolate ellipsoid of axial ratio $a/b = 3.5$, the ratio of the friction coefficients about the two axes (τ_a/τ_b) would be ~2.5, based on calculations from the Perrin equations (Edsall, 1943). No attempt was made to resolve such corresponding rotational relaxation times in the current experiments. The rotational diffusion coefficient determined here therefore represents a harmonic mean of two or more rotations about different axes. In such a case our assumption of protein sphericity would tend to underestimate the particle size. With this in mind it is apparent that our value for the radius of BSA falls well within the range of results previous reported. It should be noted though that the most precise results mentioned above were obtained for aqueous solutions of BSA. Since our studies were carried out in high concentrations of glycerol, careful hydrodynamic measurements made under similar conditions would be useful for comparison.

In summary we have presented equations predicting the absolute fluorescence recovery signals observed in PFD experiments. We have shown how various parameters of slow molecular rotational motion can be evaluated directly from PFD experimental data. Also presented are correction factors for high numerical aperture observation and equations for laser-induced heating of samples. Although neither of these factors proved to be significant in our system, they are included for future use. Experimentally we have demonstrated that the model for a spherical particle rotating in solution does satisfactorily describe our experimental observations of BSA in glycerol. In particular the linear dependence of the diffusion coefficient on sample viscosity and temperature, according to the Stokes-Einstein equations, strongly confirms both theory and instrumentation. We therefore feel that our system has been shown to measure both translational and rotational diffusion of proteins in solution with good agreement with previously published results. We believe that, as researchers apply PFD methods to cellular and membrane systems, dependable absolute values of rotational parameters can be obtained.

Supported by National Science Foundation grant PCM 84-10763 and National Institutes of Health grant AI-21873.

Received for publication 10 September 1985 and in final form 18 March 1986.

REFERENCES

Axelrod, D. 1977. Cell surface heating in fluorescence photobleaching recovery experiments. *Biophys. J.* 18:129–137.

Axelrod, D. 1979. Carbocyanine dye orientation in red cell membrane studied by microscopic fluorescence polarization. *Biophys. J.* 26:557–573.

Barisas, B. G., and M. D. Luther. 1979. Fluorescence photobleaching recovery measurements of protein absolute diffusion constants. *Biophys. Chem.* 10:221–229.

Barisas, B. G. 1980. Criticality of beam alignment in fluorescence photobleaching recovery experiments. *Biophys. J.* 29:545–548.

Cherry, R. J., A. Cogoli, M. Oppliger, G. Schneider, G. Semenza. 1976. A spectroscopic technique for measuring slow rotational diffusion of macromolecules. 1: Preparation and properties of a triplet probe. *Biochemistry.* 15:3653–3656.

Cherry, R. J., and G. Schneider. 1976. A spectroscopic technique for measuring slow rotational diffusion of macromolecules. 2: Determination of rotational correlation times of proteins in solution. *Biochemistry.* 15:3657–3661.

Damjanovich, S., L. Tron, J. Szollösi, R. Zidovetzki, W. L. C. Vaz, F. Regateiro, D. Arndt-Jovin, and T. M. Jovin. 1983. Distribution and mobility of murine histocompatibility H-2^k antigen in the cytoplasmic membrane. *Proc. Natl. Acad. Sci. USA.* 80:5985–5989.

Edelman, G. M. 1976. Surface modulation in cell recognition and cell growth. *Science (Wash. DC.).* 192:218–226.

Edsall, J. T. 1943. Rotary brownian movement. The shape of protein molecules as determined from viscosity and double refraction of flow. *In* Proteins, Amino Acids and Peptides. E. J. Cohn and J. T. Edsall, editors. Reinhold Publishing Corp., New York. Chap. 21.

Garland, P. B., and P. Johnson. 1985. Rotational diffusion of membrane

proteins (Optical methods). *In* The Enzymes of Biological Membranes. A. N. Martonosi, editor. Plenum Publishing Corp. Vol. 1. Chap. 13.

Huntz, I. D., and W. Kauzmann. 1974. Hydration of proteins and polypeptides. *In* Advances in Protein Chemistry. C. B. Anfinsen, J. T. Edsall, and F. M. Richards, editors. Academic Press Inc., New York. 28:239–345.

Jähnig, F. 1979. Structural order of lipids and proteins in membranes: Evaluation of fluorescence anisotrophy data. *Proc. Natl. Acad. Sci. USA.* 76:6361–6365.

Johnson, P., and P. B. Garland. 1981. Depolarization of fluorescence depletion. *FEBS (Fed. Eur. Biochem. Soc.) Lett.* 132(2): 252–256.

McConnell, H. M. 1975. Lateral molecular motion in membranes. *In* Functional Linkage in Biomolecular Systems. F. O. Schmitt, D. M. Schneider, and D. M. Crothers, editors. Rover Press, New York. Chap. 5.

Moore, C., D. Boxer, and P. Garland. 1979. Phosphorescence depolarization and the measurement of rotational motion of proteins in membranes. *FEBS (Fed. Eur. Biochem. Soc.) Lett.* 108:161–166.

Peacock, J. S., and B. G. Barisas. 1981. Photobleaching recovery studies of antigen-specific mouse lymphocyte stimulation by DNP-conjugated polymerized flagellin. *J. Immunol.* 127:900–906.

Peters, R. 1981. Translational diffusion in the plasma membrane of single cells as studied by fluorescence microphotolysis. *Cell Biol. Int. Rep.* 5:733–760.

Peters, R., and R. J. Cherry. 1982. Lateral and rotational diffusion of Bacteriorhodopsin in lipid bilayers: Experimental test of the Saffman-Delbrück equations. *Proc. Natl. Acad. Sci. USA.* 79:4317–4321.

Saffman, P. G., and M. Delbrück, 1975. Brownian motion in biological membranes. *Proc. Natl. Acad. Sci. USA.* 72:3111–3113.

Saffman, P. G. 1976. Brownian motion in thin sheets of viscous fluid. *J. Fluid Mech.* 73:593–602.

Segur, J. B., and H. E. Oberstar. 1951. Viscosity of glycerol and its aqueous solutions. *Ind. Eng. Chem.* 43:2117–2120.

Speirs, A., C. H. Moore, D. H. Boxer, and P. B. Garland. 1983. Segmental motion and rotational diffusion of the Ca^{2+}-translocating adenosine triphosphatase of sarcoplasmic reticulum, measured by time-resolved phosphorescence depolarization. *Biochem. J.* 213:67–74.

Squire, P. G., P. Moser, C. T. O'Konski. 1968. The hydrodynamic properties of bovine serum albumin monomers and dimer. *Biochemistry.* 7:4261–4272.

Tanford, C. 1961. Physical Chemistry of Macromolecules. John Wiley & Sons, Inc., New York. Chap. 6.

Wegener, W. A. 1984. Fluorescence recovery spectroscopy as a probe of slow rotational motions. *Biophys. J.* 46:795–803.